Finite-Element-Based Multiobjective Design Optimization Procedure of Interior Permanent Magnet Synchronous Motors for Wide Constant-Power Region Operation

Francesco Parasiliti, Marco Villani, Stefano Lucidi, and Francesco Rinaldi

***Abstract*—This paper proposes the design optimization procedure of three-phase interior permanent magnet (IPM) synchronous motors with minimum weight, maximum power output, and suitability for wide constant-power region operation. The particular rotor geometry of the IPM synchronous motor and the presence of several variables and constraints make the design problem very complicated. The authors propose to combine an accurate finite-element analysis with a multiobjective optimization procedure using a new algorithm belonging to the class of controlled random search algorithms. The optimization procedure has been employed to design two IPM motors for industrial application and a city electrical scooter. A prototype has been realized and tested. The comparison between the predicted and measured performances shows the reliability of the simulation results and the effectiveness, versatility, and robustness of the proposed procedure.**

***Index Terms*—Automotive applications, design methodology, design optimization, electric vehicles, finite-element (FE) methods, flux weakening, magnetic analysis, permanent-magnet (PM) motors, search methods, variable-speed drives.**

NOMENCLATURE

d–q	Rotating reference frame.
v_d, v_q	d–q stator voltage components.
i_d, i_q	d–q stator current components.
Φ_M	Stator flux linkage amplitude due to the magnet.
ω	Electrical speed.
R	Stator phase resistance.
L_d, L_q	$d-q$ stator synchronous inductances.
T	Electromagnetic torque.
p	Number of pole pairs.
x	Design variables.
$f(x)$	Objective function.
$g(x)$	Constraint functions.
l, u	Variables (lower and upper limits).
F	Variables feasible set.
$P(x)$	Augmented objective function.
n	Number of design variables.
k	Iteration index.
S^k	Set of points chosen randomly.
m	Number of points in S^k.
L_S	Losses per radiating slot surface.
σ	Current density.
k_s	Stator slot fill factor.
ρ	Copper resistivity.
w_s	Average slot width.
h_s	Slot height.
γ	Angle between current vector and q-axis.

Manuscript received December 23, 2010; revised April 20, 2011, May 12, 2011, May 26, 2011, and June 1, 2011; accepted June 18, 2011. Date of publication October 13, 2011; date of current version February 10, 2012.

F. Parasiliti and M. Villani are with the Department of Electrical and Information Engineering, University of L'Aquila, 67100 L'Aquila, Italy (e-mail: francesco.parasiliti@univaq.it; marco.villani@univaq.it).

S. Lucidi and F. Rinaldi are with the Department of Computer and System Sciences "Antonio Ruberti," "Sapienza" University of Rome, 00185 Rome, Italy (e-mail: lucidi@dis.uniroma1.it; rinaldi@dis.uniroma1.it).

Color versions of one or more of the figures in this paper are available online at http://ieeexplore.ieee.org.

Digital Object Identifier 10.1109/TIE.2011.2171174

I. INTRODUCTION

THE INTERIOR permanent-magnet (PM) (IPM) synchronous motors, built with magnets placed inside the rotor body, are attracting great attention in several variable-speed applications, such as electric vehicles and industrial and domestic appliances, where the most challenging requirements are high efficiency, high torque density, good overload capability, and extended speed range.

Additional features are the robustness of the rotor structure, mechanically suited to high-speed operation, and the presence of magnetic saliency: The "direct" d-axis inductance is substantially different from the "quadrature" q-axis inductance, where the d-axis is aligned with the PM flux according to the equivalent Park model of the synchronous machine. This characteristic is particularly suited for extending the torque/speed operating region by proper "field-weakening" control techniques. The most popular approach is to combine the maximum torque per ampere trajectory with the voltage-constraint-tracking field-weakening control [1]–[5]. Moreover, it allows the application of some interesting approaches to position and speed detection, namely, "self-sensing" or "sensorless" control [6]–[8].

On the other hand, IPM motors have quite strong nonlinear operating characteristics, often increased by saturation and mutual axis interaction ("cross-coupling") [9].

Then, to take advantage of the motor features, during the design stage, the performance prediction should be reliable all over the operating range. The accurate analysis of these

0278-0046/$26.00 © 2011 IEEE

Authorized licensed use limited to: Universita degli Studi di Roma La Sapienza. Downloaded on September 15,2022 at 09:42:33 UTC from IEEE Xplore. Restrictions apply.

motors requires the use of numerical techniques like the finite-element (FE) method that takes into account the remarkable saturation phenomena in certain parts of the rotor particularly if the magnets are fully buried and enclosed by the rotor core. Reference [10] shows the use of the FE method to calculate the torque, reluctance torque, back iron flux density, tooth flux density, detent torque, and back-electromotive force (emf) of IPM motors. In [11], an IPM motor was designed by using an equivalent magnetic circuit model where inductance and iron-loss resistance, which are critically affected by magnetic saturation, are obtained using FE analysis (FEA). In [12], the conventional d–q-axis mathematical model was modified in order to include data derived from 3-D FEA. Indirect interaction between FEA and circuit simulation enhances model fidelity, embodying the influence of saturation and cross-coupling effects.

Moreover, the demand of high-performance motors needs the use of a design optimization procedure in combination with suitable analytical or FE motor models, which is the most popular approach to design IPM motors in literature. Differences concern the motor model, the aim of the optimization, the design object (part or all of the motors), the requirement of an initial feasible design, and the search method.

In [13], novel rotor designs of IPM motors in order to reduce harmonic iron losses at high rotational speeds under field-weakening control were proposed. An optimization method, combined with an adaptive FE method, was applied to determine automatically the shapes of the magnets and rotor core.

Two case studies were proposed in [14]. In the first, the goal of the optimization was to obtain a back-emf with a maximal amplitude and low distortion. A coupled FE-grid-search algorithm was implemented in order to synthesize the shape of the rotor surface with only one design variable, the radius of the rotor surface. In the second, a multiobjective rotor topology optimization was presented, coupling FE calculations with genetic algorithms. The chosen objective functions were the amplitude of the phase flux linkage first harmonic and the reciprocal value of the cogging torque amplitude. The same authors in [15] proposed a multiobjective optimization design method using three different optimization algorithms (Hooke–Jeeves, genetic algorithms, and grid search). The optimizations were performed in two stages. The Hooke–Jeeves method and genetic algorithms were used for the global search, and a fine grid search was done around the optimum given by the first two methods. The efficiency and cost of the active materials and technology were considered as fitness functions. The multiobjective optimization was performed using an analytical model with embedded FE correction factors. Seven design variables were considered. Methods to reduce acoustic noise in an IPM motor during the design stage were presented in [16]. In [17], a method was proposed to design the optimal stator configurations of a traction motor of a hybrid electric vehicle to reduce torque ripples. The focus of [18] was to improve the self-sensing performance of an IPM synchronous machine by modifying the rotor configurations. A FEA has been used to design and assess the performance of the machine for self-sensing. In [19], the rotor design was discussed and used to reduce the estimation error caused by cross-saturation in the sensorless control.

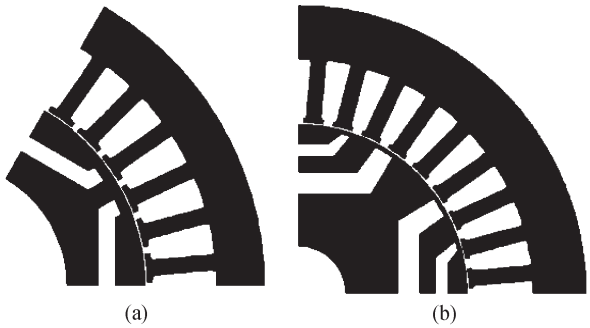

Fig. 1. Typical cross-sections of the considered IPM motors (one pole).

The objective of improving the flux-weakening capability of IPM motors received wide interest in literature. In [20], analytical models were used and validated by FE computations. The design was formulated as a constrained multiobjective optimization problem consisting of maximizing the machine efficiency while minimizing its weight. At the end of the process, the designer made an a posteriori choice. In [21], using FE simulations, the authors analyzed the method for maximizing performance by modifying the PM quantity. Reference [22] proposed the rotor design optimization of IPM motors for wide speed ranges by means of a FEA-based multiobjective genetic algorithm with three goal functions (motor torque, torque ripple, and flux-weakening capability).

This paper proposes a design optimization procedure of three-phase IPM synchronous motors suitable for wide constant-power region operation with the aim of minimizing the motor weight and maximizing the output power.

The peculiarities of the proposed approach are the following.

1) There are multiple objective functions (three), with one term conflicting with the others.
2) The optimization is performed in two distinct operating points (rated and high speed).
3) The design concerns all motors (stator and rotor cores, winding, and magnets).
4) Some of the design variables vary in a discrete way with fixed steps.
5) All motor performances are evaluated using the FE method.
6) The design procedure does not need to start from a known initial design, i.e., a feasible initial design is not required.

The proposed design optimization of the IPM motors is based on a new algorithm belonging to the class of controlled random search (CRS) algorithms that derives from the algorithm proposed in [23]. CRS algorithms follow a strategy which combines a global and a local search phase. The proposed FE-based multiobjective optimization procedure is employed to design two machines with different rotor structures: a single-barrier six-pole motor for industrial application [Fig. 1(a)] and a double-barrier four-pole motor for a city electrical scooter [Fig. 1(b)].

The conventional single-layer IPM model is the simplest solution, with a significant reduction on the manufacturing cost

Authorized licensed use limited to: Universita degli Studi di Roma La Sapienza. Downloaded on September 15,2022 at 09:42:33 UTC from IEEE Xplore. Restrictions apply.

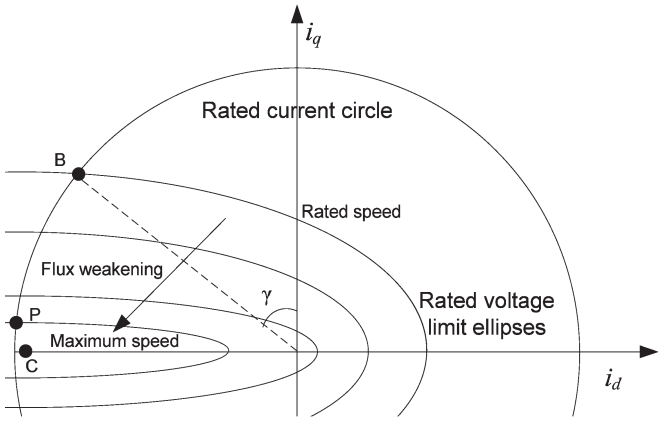

Fig. 2. Constant voltage and current loci in the d–q current plane.

with respect to the double-layer one. The second solution is popular in the recent years since its high-saliency-ratio rotor structure is beneficial for increasing the machine performance and torque quality.

II. Motor Basic Representations

The steady-state IPM motor stator voltage equations written in the d–q rotating reference frame are

$$v_d = Ri_d - \omega L_q i_q \tag{1}$$

$$v_q = Ri_q + \omega L_d i_d + \omega \Phi_M \tag{2}$$

where i_d, i_q, v_d, and v_q are the d- and q-axis components of the armature current and terminal voltage, respectively, R is the winding resistance per phase, L_d and L_q are the axis inductances, ω is the electrical speed, and Φ_M is the magnet flux linked with the d-axis armature winding.

The electromagnetic torque is calculated using the following well-known equation:

$$T = \frac{3}{2} p \left[\Phi_M i_q + (L_d - L_q) i_d i_q\right] \tag{3}$$

where p is the number of pole pairs.

Simple manipulations of the basic relations (1)–(3) provide the basic expressions of the constant voltage and current loci in the d–q current plane represented by "voltage ellipse" and "current circle," respectively (Fig. 2). At the rated condition, they share a point which is the "rated" operating point of the IPM motor (point B). For increasing speed (and fixed rated voltage), one has a family of voltage "limit" ellipses which converge to their center (point C). At that point, the speed is theoretically infinite and the torque is zero.

Above base speed, the operation is limited by the rated current and voltage and the motor is controlled by the "field-weakening" method. The operating points under these limit conditions are the intersections between the current limit circle and the voltage limit ellipses, and the current vector moves from B to P, where the speed is maximum. Because of the constant voltage constraint, the flux and, hence, the torque decrease in inverse proportion to speed.

III. Design Approach

To guarantee a wide constant-power operation, the motor requires an accurate design through the use of salient rotor geometry with limited flux contribution from PMs buried within the rotor structure. To achieve the desired degree of saliency, maximize the power density, and guarantee good performance, a special lamination profile should be found.

The particular rotor geometry of the IPM synchronous motor and the presence of several variables and constraints make the design problem very complicated to solve. A good way is to carry out a design procedure, combining accurate FEA with mathematical optimization algorithms. This paper proposes a new design approach based on this idea.

The study concerns the design of the following two IPM synchronous motors.

1) A 5-kW 6-pole 36-slot motor for industrial application (M1 motor). The chosen rotor presents one barrier per pole, and the magnet material is inserted into this cavity.
2) A 4-kW 4-pole 36-slot motor for a city electrical scooter (M2 motor). The rotor presents two magnet layers per pole, a choice that provides higher saliency ratio than the single-layer design. The design constraints are in compliance with a conventional 100 cc scooter for two passengers with a rated speed of 30 km/h and a maximum speed of 70 km/h.

The choice of different numbers of barriers results from the applications and costs. The IPM synchronous motor guarantees high torque generation at constant current and wide speed operating range if the q-axis inductance is high [24], [25]. This can be obtained, for a constant magnet volume, by splitting up each rotor pole in two (or more) PM cavity layers with iron separation in the radial direction to increase the anisotropy in the magnetic path, thereby enhancing the saliency. However, the addition of one more cavity increases the complexity in the rotor construction and its manufacturing cost.

The stator and rotor consist of a stack of laminated high-permeability nonoriented grain silicon steel: 330–50 and 330–35 AP for M1 and M2, respectively. Three-phase double-layer distributed windings are inserted in the stator slots. NdFeB magnets are chosen due to their high energy density. The remanent flux density B_r at 20 °C is 1.16 T, and the coercive field strength H_c is 900 kA/m.

A temperature of 90 °C is considered for the stator windings and 75 °C for the PMs. These values have been chosen taking into account the cooling systems of the considered machines: liquid cooled for M1 and air-forced cooled for M2. These efficient systems guarantee a maximum operating temperature in the stator windings usually below $80 \div 90$ °C.

The IPM synchronous motors are modeled using FE "parametric models" that allow the variation of the geometric dimension of motor, current distribution, and rotor position. Torque prediction is carried out for several stator–rotor relative positions, and the FE grid is automatically adjusted when the rotor is rotated. The influence of a mesh has been investigated in order to get satisfactory accuracy, avoiding the inaccuracies due to the element distortion. Only one pole is simulated, because of the motor symmetries.

Authorized licensed use limited to: Universita degli Studi di Roma La Sapienza. Downloaded on September 15,2022 at 09:42:33 UTC from IEEE Xplore. Restrictions apply.

TABLE I
OPERATING POINTS

Motor			M1	M2
	Rated voltage	V	150	44
	Rated current	A	30	90
Point B (base speed)	Current vector angle γ	deg.	35	45
	Speed	rpm	4000	2600
Point P (high speed)	Current vector angle γ	deg.	85	80
	Speed	It depends on the optimization		

TABLE II
DESIGN M1: MINIMUM AND MAXIMUM RANGES OF DESIGN VARIABLES

Discrete variables		min	max	step
x1. Stack length	mm	60	90	1
x2. Outer stator diameter	mm	100	130	1
x14. Angle of flux barrier	deg.	-10	10	1
x15. Angle of flux barrier	deg.	-10	10	1
x17. Number of wires per slot		4	14	1
x18. Wire size	mm	1.0	2.0	0.05
Continuous variables		min	max	-
x3. Inner stator diameter	mm	72	80	-
x4. Stator tooth width	mm	2.0	3.0	-
x5. Stator yoke thickness	mm	3.0	5.0	-
x6. Slot opening width	mm	1.2	1.6	-
x7. Slot opening depth	mm	1.0	2.0	-
x8. Bottom loop radius	mm	0.3	0.8	-
x9. Upper loop radius	mm	0.3	0.8	-
x10. PM thickness	mm	2.0	4.0	-
x11. Ratio of PM width to barrier width		0.80	0.95	-
x12. Magnet position	mm	4.0	8.0	-
x13. Rotor tooth width	mm	4.0	6.0	-
x16. Thickness of steel bridge	mm	2.0	3.0	-

TABLE III
DESIGN M2: MINIMUM AND MAXIMUM RANGES OF DESIGN VARIABLES

Discrete variables		min	max	step
x1. Stack length	mm	90	130	1
x13. Angle of flux barrier	deg.	-10	10	1
x14. Angle of flux barrier	deg.	-10	10	1
x15. Number of wires per slot		1	10	1
x16. Wire size	mm	1.0	5.0	0.05
Continuous variables		min	max	-
x2. Stator tooth width	mm	2.5	5.0	-
x3. Stator yoke thickness	mm	4.0	10.0	-
x4. Slot opening width	mm	1.5	2.5	-
x5. Inner PM position	mm	6.0	12.0	-
x6. Inner PM thickness	mm	2.0	8.0	-
x7. Distance between PMs	mm	2.0	10.0	-
x8. Outer PM thickness	mm	2.0	5.0	-
x9. Ratio of inner PM width to barr. width		0.8	0.95	-
x10. Ratio of outer PM width to barr. width		0.8	0.95	-
x11. Thickness of steel bridge	mm	1.0	3.0	-
x12. Rotor tooth width	mm	5.0	15.0	-

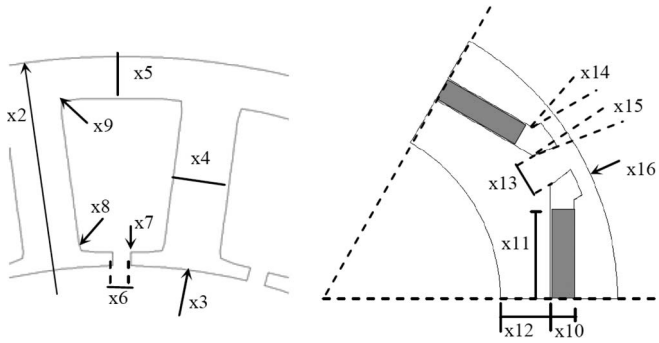

Fig. 3. Design M1. Variables.

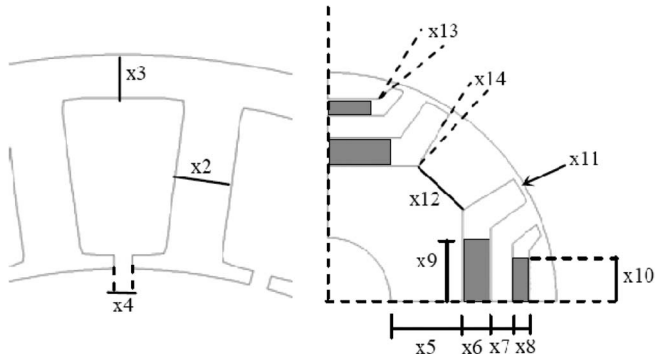

Fig. 4. Design M2. Variables.

The input data of the FE model are the motor geometry and the $d-q$ axis currents. By means of an out-of-line procedure, the phase currents are assigned to each slot. The motor torque is calculated by Virtual Work principle.

The qualitative aim of the optimization is to maximize the torque at the base and high speeds, to extend the flux weakening region and to minimize the motor weight. The aim is pursued by a multiobjective optimization procedure with the following objectives:

1) maximize the torque at base speed (point B, Fig. 2);
2) maximize the torque at maximum speed (point P, Fig. 2);
3) minimize the weight of the motor.

The optimization is performed in the operating points B and P corresponding to the values shown in Table I.

The voltage values are chosen according to the applications. The current amplitude and vector angle γ are defined based on a preliminary study [26]. In B, speed is calculated based on voltage, current, and angle values. In P, speed depends on the optimization because it is "constrained" to be higher than a chosen value (see Table IV), i.e., as high as possible (maximum).

The design variables concern the stator and rotor cores, PM size, and stator winding. The rotor shape should be designed in order to have, in addition to the PM torque, a torque component due to the anisotropy of the rotor. An accurate design of the flux barriers can increase the difference between the reluctance of the d- and q-axes, thus increasing the reluctance torque component and improving the motor performance when it is driven at constant power over a wide speed range.

The set of variables $\boldsymbol{x}$ used in the optimization procedure are listed in Tables II and III, with their limits, and shown in Figs. 3 and 4.

The limits on the design variables have been chosen in order to guarantee the feasibility of the final designs. The wide ranges of these "box constraints" and the high number of variables and constraints make the optimization problem very complicated and could require significant computational effort. However, these allow the authors to define, in detail, a reliable final design.

Authorized licensed use limited to: Universita degli Studi di Roma La Sapienza. Downloaded on September 15,2022 at 09:42:33 UTC from IEEE Xplore. Restrictions apply.

TABLE IV
CONSTRAINTS

Constraints		M1	M2
c1. Stator slot fill factor		≤ 0.40	≤ 0.40
c2. Max flux density in the stator tooth	T	≤ 1.80	≤ 1.80
c3. Max flux density in the stator yoke	T	≤ 1.80	≤ 1.80
c4. Linear current density (rms)	A/cm	≤ 400	≤ 400
c5. Efficiency @ base speed	%	≥ 90	≥ 90
c6. Maximum speed	rpm	≥ 20000	≥ 6000
c7. Back EMF @ maximum speed	V	≤ 120	≤ 40

TABLE V
CONSTANT QUANTITIES

		M1	M2
air gap length	mm	0.5	0.4
inner rotor diameter D_{ir}	mm	50	24
outer stator diameter	mm	-	130

Design M1 has 18 variables. Among these, six variables (stack length, outer stator diameter, number of wires per slot, wire size, and flux barrier angles) vary in discrete ways.

Design M2 has 16 variables. Among these, five variables (stack length, number of wires per slot, wire size, and flux barrier angles) vary in discrete ways. The outer stator diameter is fixed according to the available space for the motor housing inside the scooter.

In this paper, fixed steps have been chosen for the discrete variables, but in a manufacturing environment, these increments can be varied according to normalized values (particularly for the stack length, outer diameter, and wire size). For good electromagnetic performance, it should be necessary to minimize the steel bridges surrounding the magnetic cavities. On the other hand, the centrifugal force on steel bridges should be taken into account, being the dominant source of mechanical stress in high-speed operation. From a preliminary analysis, a minimum value of 2 mm has been imposed for M1 and 1 mm for M2. These values are consistent with the maximum speed and mechanical stress.

The design optimization needs to satisfy several constraints to guarantee the reliability and feasibility of the final design. The considered constraints are listed in Table IV.

The flux density value in the stator yoke is slightly higher than the typical values [25], but for the proposed applications, it is reasonable, owing to the use of a high-permeability core material.

The efficiency has been calculated as ratio between the output power and the output power plus total losses.

The optimization has been carried out by imposing a constant value of the current vector, 30 A for design M1 and 90 A for design M2. By a preliminary analysis, the demagnetization of the magnets has been checked at the same negative direct-current values with a PM minimum thickness of 2.0 mm.

The quantities fixed during optimization are shown in Table V.

The magnetostatic FEA is used to evaluate the motor performance and the design requirements (at base and maximum speeds), namely, to compute the objective function values and constraints of the minimization problem which mathematically represents the optimal design problem. The optimization procedure uses the information obtained by the FE program to update the set of motor parameters iteratively and try to identify an "optimal" motor by making a tradeoff between the different parameters of the machine.

IV. OPTIMIZATION ALGORITHM

As described before, the optimal design problem of an IPM synchronous motor can be formulated as a particular multiobjective mixed-integer nonlinear programming problem. Its main features are the following.

1) There are multiple objective functions that are conflicting with each other. This means that an improvement in one of them induces a worsening of at least one of the others.
2) Some of the variables of the problem vary in a discrete way with fixed steps, and this implies that the ratio between these variables and their steps must assume integer values.

In this paper, the authors focus on defining an algorithm which efficiently tackles the mixed-integer aspect of the problem since it appears to be crucial for the considered design problem.

With regards the multiobjective aspect of the optimization problem, the authors' experience showed that, for this particular optimal design problem, a good compromise among different objectives can be obtained just by minimizing the sum of the weight of the motor and the opposites of the two torques.

Therefore, the general structure of the considered optimization problem is as follows:

$$\begin{aligned} &\min f(x) \\ \text{s.t.}\quad &g(x) \le 0 \\ &l \le x \le u \\ &x_i \in Z, \quad i \in I_z \end{aligned} \tag{4}$$

where Z is the set of the integer numbers, $x \in R^n$, f: $R^n \to R$, g: $R^n \to R^m$, $l, u \in R^n$, $l_i, u_i \in Z$, and $i \in I_z$.

The set

$$F = \{x \in R^n : g(x) \le 0,\ l \le x \le u\}$$

is called a feasible set.

However, the motor design problem has the following further distinguishing features that make it difficult to solve.

1) The optimization problem may have different local minimum points besides the global one.
2) Explicit mathematical representations of the objective and constraint functions are not available; therefore, the first-order derivatives of f and g_i cannot be explicitly calculated or approximated.
3) The objective function may not be available or defined when the point is unfeasible (i.e., the point does not satisfy the constraints).
4) The constraints are highly nonlinear and tight, an initial feasible design is not known, and/or it is difficult to find a feasible point and keep the feasibility once it has been gained.

Authorized licensed use limited to: Universita degli Studi di Roma La Sapienza. Downloaded on September 15,2022 at 09:42:33 UTC from IEEE Xplore. Restrictions apply.

The authors decided to tackle the feasibility issue by means of an exact penalization of the constraints [27], [28]. Roughly speaking, the nonlinearly constrained problem is converted into a box-constrained one by adding to the objective function a term which penalizes the nonlinear constraint violations, i.e., "the augmented objective function"

$$P(x) = f(x) + \frac{1}{\varepsilon}\max\{0, g_1(x), \ldots, g_m(x)\}$$

where $\varepsilon = 10^{-1}$ is the penalty parameter.

Then, the following mixed-integer box-constrained problem is considered:

$$\begin{aligned} &\min P(x) \\ \text{s.t.} \quad &l \le x \le u \\ &x_i \in Z,\ i \in I_z. \end{aligned} \tag{5}$$

In order to solve problem (5) efficiently, a new algorithm belonging to the class of CRS algorithms has been proposed. This class derives from the original algorithm described in [29], and it has been proven to be useful and effective in solving several global optimization problems deriving from real-world applications [30]–[33]. Similarly to other global optimization methods, CRS algorithms follow a strategy which combines a global and a local search phase. The global search is used to locate the subregions that are "more promising" to contain a global minimizer. The local search is used for determining the global minimizer as soon as a "sufficiently small" neighborhood of this point has been located.

The basic idea of CRS methods is to generate an initial set of points in the box $l \le x \le u$ randomly and to update this sample iteratively by substituting the worst point, in terms of objective function value, with a better one obtained by a local search. In this way, the set of sample points should cluster more and more around the subregions, which are more likely to contain a global minimizer. Therefore, these methods follow an approach which can be considered a compromise between a pure random-search and a clustering strategy derived by a deterministic local search.

In order to solve the mixed-integer nonlinear programming problem (5), the authors propose a modification of the algorithm proposed in [23], which directly handles the discrete variables with a reasonable computational effort.

Optimization Algorithm (OA)
Data: **Set** $m = 25n$ and $k = 0$
where n is the number of variables, m is the number of points in S_k and k is the iteration index.
Step 0: **Determine** $S^k = \{x_1^k, \ldots\ldots x_m^k\}$ a set of points chosen at
random over $l \le x \le u$ and
Compute $P(x_{\max}^k) = \max_{x \in S^k} P(x)$
and $P(x_{\min}^k) = \min_{x \in S^k} P(x)$.
While (*stopping criterion* is not satisfied) **do**
Choose $n+1$ points over S^k with a *weighted random procedure* and rename these points as

$$x_{i_1}^k, \ldots, x_{i_n}^k, x_{i_{n+1}}^k$$

with $P(x_{i_{n+1}}^k) \ge P(x_{i_j}^k)$, $j = 1, \ldots\ldots, n$.
Compute the trial point $\tilde{x}^k$ by

$$\tilde{x}^k = c^k - \alpha^k\left(x_{i_{n+1}}^k - c^k\right)$$

where

$$c^k = \sum_{j=1}^{n+1} w_j^k x_{i_j}^k$$

$$\alpha^k = 1 - \frac{P\left(x_{i_{n+1}}^k\right) - \sum_{j=1}^{n+1} w_j^k P\left(x_{i_j}^k\right)}{P\left(x_{\max}^k\right) - P\left(x_{\min}^k\right) + \phi^k}$$

with

$$w_j^k = \frac{\eta_j^k}{\sum_{j=1}^{n+1}\eta_j^k},$$

$$\eta_j^k = \frac{1}{P\left(x_{i_j}^k\right) - P\left(x_{\min}^k\right) + \phi^k},$$

$$\phi^k = 10^3\frac{\left(P\left(x_{\max}^k\right) - P\left(x_{\min}^k\right)\right)^2}{P\left(x_{\max}^0\right) - P\left(x_{\min}^0\right)}.$$

Discretize each variable $(\tilde{x}^k)_d$ whose index d belongs to the set I_z

$$(\tilde{x}^k)_d = \left\lfloor \frac{(\tilde{x}^k)_d}{s_d} + \frac{1}{2}\right\rfloor s_d, \quad d \in I_z$$

where s_d is the step of the variable $(x)_d$.
If $\tilde{x}^k \in F$ and $f(\tilde{x}^k) \le f_{\max}^k$
then
Set $S^{k+1} = S^k \bigcup \{\tilde{x}^k\} \setminus \{x_{\max}^k\}$
Determine $P(x_{\max}^{k+1}) = \max_{x \in S^{k+1}} P(x)$ and

$$P\left(x_{\min}^{k+1}\right) = \min_{x \in S^{k+1}} P(x).$$

Else
Set $S^{k+1} = S^k$, $x_{\min}^{k+1} = x_{\min}^k$, $x_{\max}^{k+1} = x_{\max}^k$
End if
Set $k = k+1$
End while

The description of the algorithm is completed by the following procedures which specify the *weighted random procedure* for determining $n+1$ points over the set S^k and the *stopping criterion* for terminating the algorithm.

Weighted Random Procedure
Data: A set $S^k = \{x_1^k, \ldots\ldots, x_m^k\}$ such that

$$P\left(x_i^k\right) \le P\left(x_{i+1}^k\right), \quad i = 1, \ldots\ldots, m-1.$$

For $j := 1, \ldots\ldots, n+1$**do**
Repeat:
generate a random number r_j uniformly distributed in [0,1] and compute $i_j = (2^{r_j} - 1)m$
Until $i_j \ne i_l$, $l = 1, \ldots, j-1$

Authorized licensed use limited to: Universita degli Studi di Roma La Sapienza. Downloaded on September 15,2022 at 09:42:33 UTC from IEEE Xplore. Restrictions apply.

End for

Select the set $\{x_{i_1}^k, \ldots x_{i_n}^k, x_{i_{n+1}}^k\}$ such that the point $x_{i_j}^k, j = 1, \ldots, n+1$, is the i_jth element of the set S^k.

Stopping criterion

Data: A set $S^k = \{x_1^k, \ldots\ldots, x_m^k\}$ such that $P(x_i^k) \leq P(x_{i+1}^k), \quad i = 1, \ldots\ldots, m-1,$ and set $\tilde{m} = 10n$.

If $(P(x_{\tilde{m}}^k) - P(x_1^k))/P(x_1^k) \leq 10^{-4}$

Stop.

V. Comments to the Optimization Algorithm

The algorithm produces a sequence S_k of sets of m points. Initially $(k = 0)$, the set S^k is randomly chosen from the set $l \leq x \leq u$, and then, it is iteratively updated so as to include points which are better estimates of the global minimizers. In particular, at each iteration, the algorithm tries to "improve" the set S^k by replacing the point of the set S^k corresponding to the biggest function value with a new point where the objective function value is improved. The search of such a point is performed by using the information contained in set S^k. In particular, the following are performed.

1) $n+1$ points are chosen over the set S^k by using a weighted random procedure which privileges the points corresponding to smaller objective function values.
2) Among these points, the point $x_{i_{n+1}}^k$ with the biggest function value is selected.
3) The weighted centroid c^k of the selected $n+1$ points $x_{i_1}^k, \ldots, x_{i_n}^k x_{i_{n+1}}^k$ is computed.
4) The new trial point $\tilde{x}^k$ is obtained by performing a suitable movement from c^k along the direction $c^k - \tilde{x}_{i_{n+1}}^k$.

The strategy for computing point $\tilde{x}^k$ is based on the idea that the function values computed at the selected $n+1$ points should give a good representation of the local behavior of the objective function around the point c^k. Therefore, in the point c^k, the vector $c^k - x_{i_{n+1}}^k$ should identify a good descent direction of the objective function, namely, a direction along which the function should decrease, at least locally.

Detailed discussions and descriptions of the formulas which define the weights w_j^k, $j = 1, \ldots, n+1$, and the step size α^k in the weighted reflection is in [23], [30], and [31]. Here, it is good to recall that, at the initial iterations (when $\phi^k \gg f(x_{i_j}^k) - f_{\min,}^k w_j^k \approx 1/(n+1),\ j = 1, \ldots, n+1$ and $\alpha_k \approx 1$), these formulas are such that the weighted centroids and the new trial point are produced without privileging any particular point $x_{i_1}^k, \ldots, x_{i_{n+1}}^k$. As the number of iterations increases, the centroid is defined by weighting the points more and more with smaller function values and the trial point is produced closer and closer to such points.

Finally, we note that the proposed algorithm does not need a (feasible) starting point. It produces a sequence S^k of sets of points starting from an initial set S^0. The points of S^0 are usually chosen at random on the set $l \leq x \leq u$. However, if one or more interesting points are known, the algorithm can exploit this information by including these points in the initial set S^0.

TABLE VI
Optimized Design M1

Stack length	82	mm
Outer stator diameter	118	mm
Inner stator diameter	76.2	mm
PM thickness	2.10	mm
Magnet position	5.81	mm
Ratio of PM width to barrier width	0.89	
Thickness of steel bridge	2.0	mm
Number of wires per slot	12	
Wire size	1.75	mm
Stator slot fill factor	0.377	
Iron gross Weight	7.0	kg
Copper Weight	1.88	kg
PM Weight	0.19	kg
Phase current (peak value)	30.0	A
Linear current density (rms)	361	A/cm
Base speed	4000	rpm
Efficiency @ base speed	92.0	%
Torque @ base speed	12.3	N·m
Output power @ base speed	5151	W
Maximum speed	24000	rpm
Torque @ max. speed	2.4	N·m
Output power @ max. speed	6031	W
Losses per radiating slot surface	10.4	W/dm^2

Fig. 5. Stator and rotor shapes (one pole) of the optimized design M1.

VI. Results

The proposed approach has been employed for the design optimization of two IPM synchronous motors in order to maximize the torque at base and high speeds, extend the flux weakening region, minimize the motor weight, and satisfy a set of constraints. No initial feasible designs were requested because the optimization procedure does not need to start from a known initial design.

The Optimization Algorithm has been implemented in Fortran 90. The FEA has been performed by ANSYS Rev. 11. All the numerical results have been obtained on an Intel Core2 duo 2.66-GHz CPU with a 1.96-GB main memory.

A. Design M1

The main data and simulation results of the optimized design are presented in Table VI. It includes some of the key machine dimensions and performance at base and maximum speeds.

The cross-section of the optimized design is shown in Fig. 5. The optimization required about 13 000 objective function calls by FEA. For each call, two operating points have been tested (at base and maximum speeds).

Authorized licensed use limited to: Universita degli Studi di Roma La Sapienza. Downloaded on September 15,2022 at 09:42:33 UTC from IEEE Xplore. Restrictions apply.

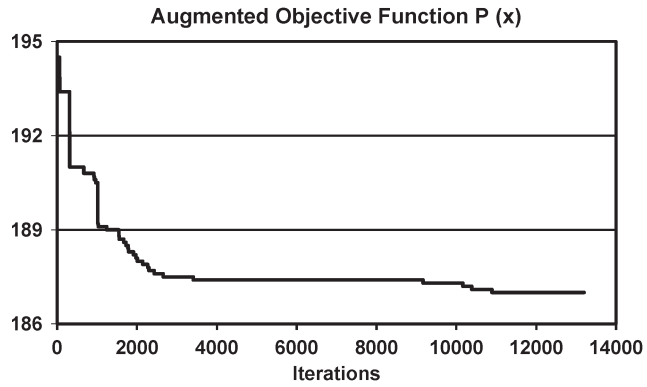

Fig. 6. Design M1. Progress of the augmented objective function versus iterations.

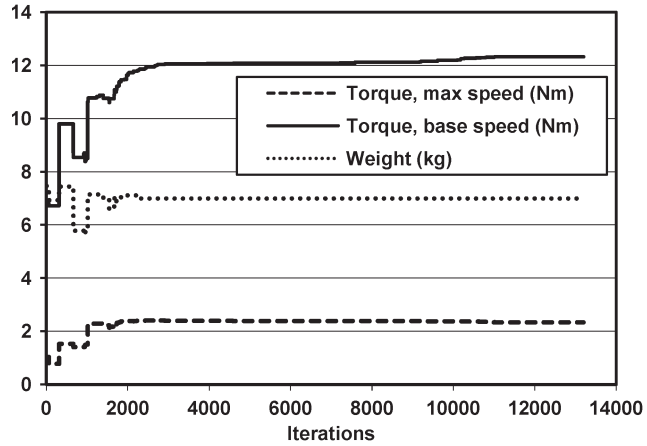

Fig. 7. Design M1. Progress of the single objective functions versus iterations.

Figs. 6 and 7 show the trend of the augmented objective function $P(x)$ (sum of the weight of the motor and the opposites of the two torques) and the single objective functions versus iterations.

The accurate motor design optimization has allowed the authors to maximize the torque while keeping down the weight of active materials without oversizing the machine. The slot fill factor value is very close to the boundary, and it guarantees the feasibility of the stator windings. At base speed (4000 r/min), the efficiency is satisfactory if it exceeds 90% and the torque is higher than 12 N · m. In the flux-weakening operation, the optimized design presents a torque of 2.4 N · m at the maximum speed of 24 000 r/min. The back-emf is widely satisfied. The maximum flux densities in the stator tooth and yoke are 1.74 and 1.80 T, respectively.

The thermal performance has been checked by introducing the specific losses, i.e., losses per radiating slot surface

$$L_S = \frac{\rho k_r w_s \sigma^2}{2\left(\frac{w_s}{h_s}+1\right)}$$

where σ is the current density, k_s the stator slot fill factor, ρ the copper resistivity (at reference temperature of 90 °C), w_s the average slot width, and h_s the slot height.

In motor M1, the losses per radiating slot surface are 10.4 W/dm^2 and assure good machine thermal performance.

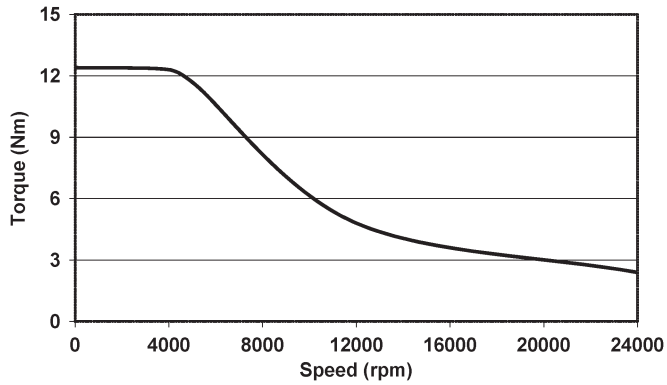

Fig. 8. Design M1. Calculated torque versus speed characteristic.

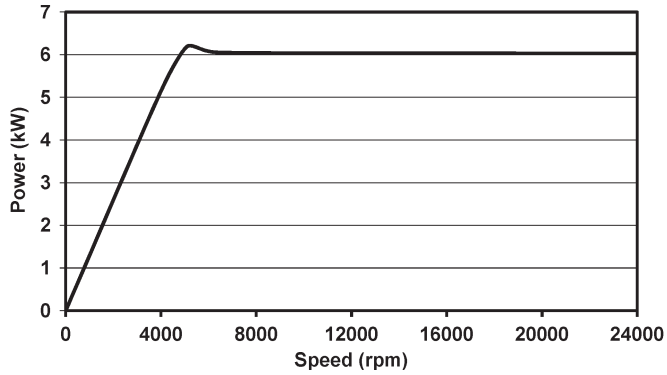

Fig. 9. Design M1. Calculated output power versus speed characteristic.

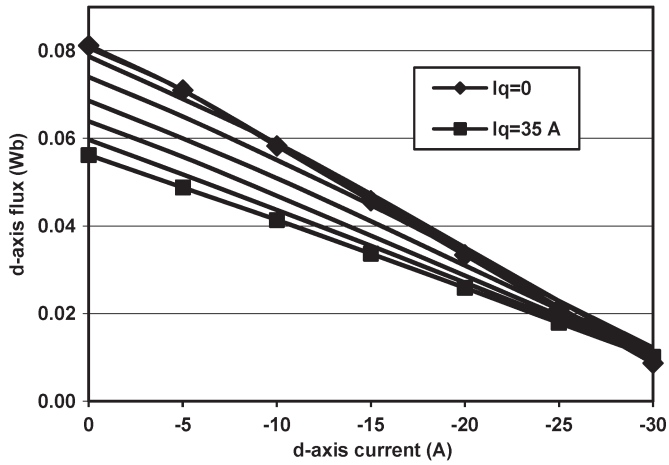

Fig. 10. Design M1. d-axis flux versus d current at a different q current.

Figs. 8 and 9 show the calculated torque-versus-speed and output power-versus-speed characteristics from the FE analyses by imposing the current trajectory (current circle) described in Section II.

The motor has excellent field-weakening performance. It is evident that the constant-power speed range is wide and the goal of our study has been fully satisfied.

Figs. 10 and 11 show the FE-calculated variation of the d- and q-axis fluxes for the different values of i_d and i_q, respectively.

Authorized licensed use limited to: Universita degli Studi di Roma La Sapienza. Downloaded on September 15,2022 at 09:42:33 UTC from IEEE Xplore. Restrictions apply.

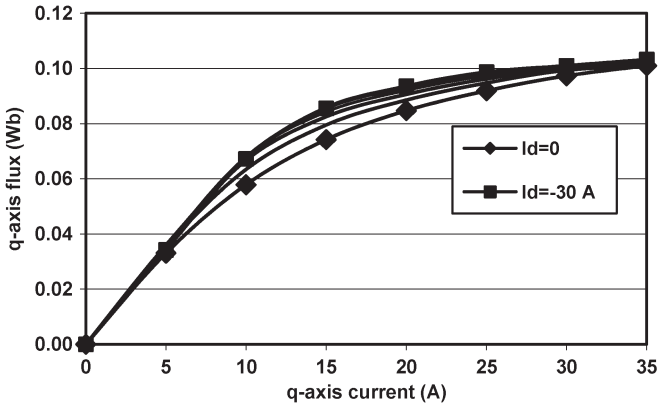

Fig. 11. Design M1. q-axis flux versus q current at a different d current.

TABLE VII
OPTIMIZED DESIGN M2

Stack length	115	mm
Inner PM thickness	5.0	mm
Outer PM thickness	2.3	mm
Inner PM position	9.2	mm
Thickness of steel bridge	1.2	mm
Number of wires per slot	3	
Wire size	3.10	mm
Stator slot fill factor	0.392	
Iron gross Weight	12.0	kg
Copper Weight	2.03	kg
PM Weight	0.51	kg
Phase current (peak value)	90.0	A
Linear current density (rms)	260	A/cm
Base speed	2600	rpm
Efficiency @ base speed	91.0	%
Torque @ base speed	17.0	Nm
Output power @ base speed	4628	W
Maximum speed	8000	rpm
Torque @ max. speed	6.3	Nm
Output power @ max. speed	5278	W
Losses per radiating slot surface	8.3	W/dm^2

Fig. 10 shows the nearly linear effect of the d-axis current and the cross-saturation effect due to the q-axis current, decreasing with increasing the demagnetizing d-axis current.

Fig. 11 shows the nonlinear effect of the q-axis current on the q-axis flux and the limited cross-saturation effect due to the d-axis current.

B. Design M2

The main data and simulation results of the motor are presented in Table VII. It includes some of the key machine dimensions and the performance at base and maximum speeds. At base speed (2600 r/min), the rated torque is 17 N · m and the efficiency is 91%. The obtained maximum speed is 8000 r/min (constraint at 6000 r/min), where the torque is 6.3 N · m. The maximum flux density in the teeth and yoke do not exceed 1.7 T, whereas it is about 1.5 T in the rotor tooth. Thermal performance are guaranteed by the low value of losses per radiating slot surface (8.3 W/dm^2).

The optimization required about 12 000 objective function calls by FEA.

Fig. 12. Design M2. View of the prototype.

Fig. 13. Design M2. Rotor lamination.

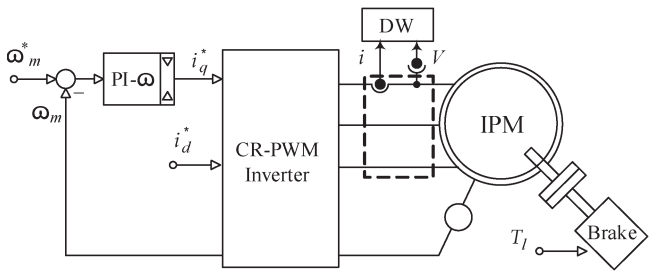

Fig. 14. Setup for experimental characterization.

Based on the optimized design, a prototype has been realized (Fig. 12). The rotor lamination of the optimized design is shown in Fig. 13.

Fig. 14 shows the experimental setup used to characterize the performance of the manufactured prototype and verify the design optimization. It includes the IPM prototype, a current-regulated vector-controlled drive, and a brake. The motor is speed controlled through a proportional–integral controller. The output of the speed controller works as the q-current (torque) reference, whereas the d-current reference can be freely imposed by the user. The brake allows setting the value of the load torque (T_l) in each test, whereas a digital wattmeter allows for the measurement of phase currents, voltages, and input power.

Authorized licensed use limited to: Universita degli Studi di Roma La Sapienza. Downloaded on September 15,2022 at 09:42:33 UTC from IEEE Xplore. Restrictions apply.

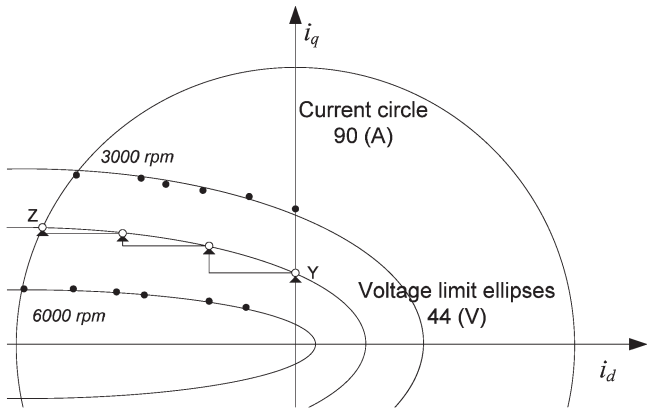

Fig. 15. Design M2. Evaluation of the $d-q$ currents along voltage limit ellipses at different speeds at flux weakening. Experimental results at 3000 and 6000 r/min.

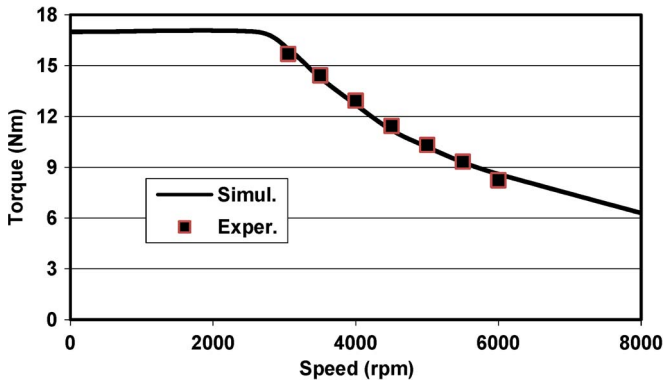

Fig. 16. Design M2. Comparisons between FE-simulated and experimental torque versus speed characteristics.

The basic goal of the characterization has been the evaluation of the $d-q$ currents along the voltage limit ellipses at different speeds at flux weakening, e.g., curve YZ in Fig. 15.

The procedure starts by setting the reference speed with the d-current reference at zero. By increasing the load, the action of the speed regulator increases the (torque) q-current until the voltage reaches the maximum (point Y). By setting a proper step of variation for the d current and load, the subsequent operating points track the voltage limit ellipse, as shown in Fig. 15. At point Z, the maximum torque is achieved at maximum current and voltage. Such "increasing load" tests, repeated all over the flux-weakening region, allow the identification of the motor performance at constant current (current circle) and at maximum voltage (voltage limit ellipses). Fig. 15 shows the experimental operating points along the voltage ellipses at 3000 and 6000 r/min.

The operating points on the current circle at variable speed are shown in Figs. 16–19, as torque, output power, d–q currents, and efficiency (direct method) versus speed, in comparison with the simulation results.

These results confirm the reliability of the simulation and the effectiveness, versatility, and robustness of the proposed procedure.

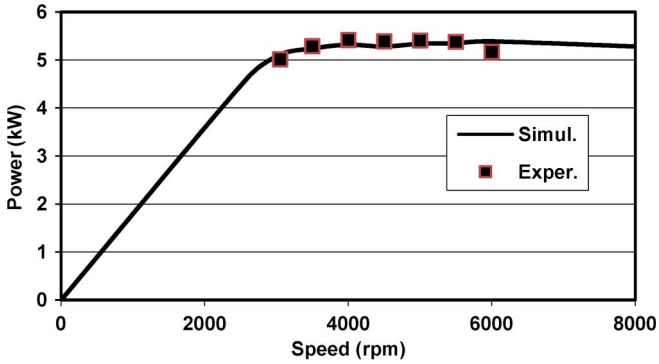

Fig. 17. Design M2. Comparisons between FE-simulated and experimental output power versus speed characteristics.

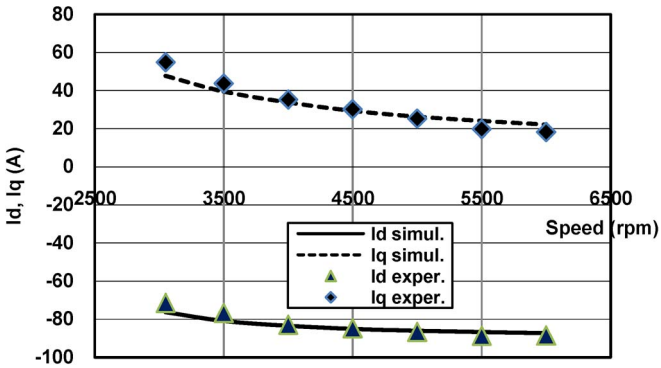

Fig. 18. Design M2. Comparisons between FE-simulated and experimental $d-q$ currents versus speed characteristics.

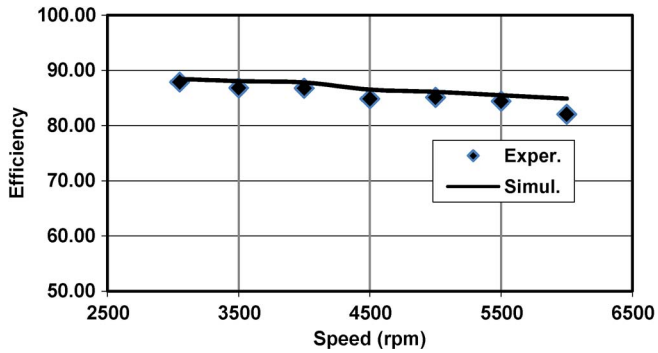

Fig. 19. Design M2. Comparisons between FE-simulated and experimental efficiency versus speed characteristics.

VII. Conclusion

The authors propose a procedure for designing IPM synchronous motors with minimum weight, maximum output power, and suitability for wide constant-power region operation. The design problem has the following main features.

1) The rotor geometry is complex with high magnetic nonlinearity.
2) The design concerns all the motor dimensions (stator and rotor cores, winding, and magnets).
3) The design is evaluated in two distinct operating points (rated and high speeds).
4) It has several continuous and discrete variables.
5) It has several, highly nonlinear, and tight constraints.

Authorized licensed use limited to: Universita degli Studi di Roma La Sapienza. Downloaded on September 15,2022 at 09:42:33 UTC from IEEE Xplore. Restrictions apply.

6) It has multiple objectives, with one term conflicting with the others.
7) Objective and constraint functions cannot be explicitly calculated or approximated.
8) It has different local minimum points besides the global one.
9) An initial feasible design may not be known, and feasibility is difficult to keep once gained.

The problem has been formulated as a particular multiobjective mixed-integer nonlinear programming problem. The multiobjective aspect of the optimization problem has been approached by minimizing the sum of the conflicting objectives, whereas the feasibility issue has been tackled by means of an exact penalization of the constraints, i.e., adding to the objective function a term which penalizes the nonlinear constraint violation.

The design problem has been solved by using a new algorithm proposed by the authors. It belongs to the class of CRS algorithms and directly handles the discrete variables with reasonable computational effort.

The algorithm does not need a (feasible) starting point and combines a global and a local search phase.

The remarkable saturation phenomena due to the buried magnets in the rotor have been taken into account by FEA which has been used to evaluate all motor performances.

To test the proposed optimization procedure, two case studies have been considered: the design of an IPM motor for industrial application and the design of an IPM motor for city electrical scooter. In the sample applications, the authors decided to consider the two cases without an initial design; hence, it is not possible to compare the final with the initial designs. This is not a lack of the procedure but is one of its peculiarities.

In conclusion, the results reported in this paper show the importance of using optimization procedures in the context of motor design. In fact, even if the considered optimization problem is a global one and the final designs cannot be defined as the "best" ones, the proposed method appears to be quite interesting. From a mathematical point of view, the final designs guarantee the satisfaction of the constraints in the model and represent a good solution in terms of objective function value. The sample applications and the prototype demonstrate that the optimization and simulation results are reliable and indirectly confirm the procedure.

REFERENCES

[1] A. Guerriero, F. Parasiliti, and M. Tursini, "Optimum vector control of high efficiency interior PM synchronous motor," in *Proc. 5th Int. Conf. Energy Efficiency Motor Driven Syst., (EEMODS'07)*, Beijing, China, Jun. 10–13, 2007, [CD-ROM].

[2] S.-M. Sue and C.-T. Pan, "Voltage-constraint-tracking-based field-weakening control of IPM synchronous motor drives," *IEEE Trans. Ind. Electron.*, vol. 55, no. 1, pp. 340–347, Jan. 2008.

[3] M. N. Uddin and M. A. Rahman, "High-speed control of IPMSM drives using improved fuzzy logic algorithms," *IEEE Trans. Ind. Electron.*, vol. 54, no. 1, pp. 190–199, Feb. 2007.

[4] B. Cheng and T. R. Tesch, "Torque feedforward control technique for permanent-magnet synchronous motors," *IEEE Trans. Ind. Electron.*, vol. 57, no. 3, pp. 969–974, Mar. 2010.

[5] C. Jo, J.-Y. Seol, and I.-J. Ha, "Flux-weakening control of IPM motors with significant effect of magnetic saturation and stator resistance," *IEEE Trans. Ind. Electron.*, vol. 55, no. 3, pp. 1330–1340, Mar. 2008.

[6] F. Parasiliti, R. Petrella, and M. Tursini, "Speed sensorless control of an interior PM synchronous motor," in *Proc. IEEE Ind. Appl. Conf.*, Pittsburgh, PA, Oct. 13–18, 2002, pp. 657–664.

[7] S.-Y. Kim and I.-J. Ha, "A new observer design method for HF signal injection sensorless control of IPMSMs," *IEEE Trans. Ind. Electron.*, vol. 55, no. 6, pp. 2525–2529, Jun. 2008.

[8] G. Foo and M. F. Rahman, "Sensorless direct torque and flux-controlled IPM synchronous motor drive at very low speed without signal injection," *IEEE Trans. Ind. Electron.*, vol. 57, no. 1, pp. 395–403, Jan. 2010.

[9] F. Parasiliti and P. Poffet, "A model for saturation effects in high-field permanent magnet synchronous motors," *IEEE Trans. Energy Convers.*, vol. 4, no. 3, pp. 487–494, Sep. 1989.

[10] L. Parsa and L. Hao, "Interior permanent magnet motors with reduced torque pulsation," *IEEE Trans. Ind. Electron.*, vol. 55, no. 2, pp. 602–609, Feb. 2008.

[11] J. Hur, "Characteristic analysis of interior permanent-magnet synchronous motor in electrohydraulic power steering systems," *IEEE Trans. Ind. Electron.*, vol. 55, no. 6, pp. 2316–2323, Jun. 2008.

[12] P. E. Kakosimos and A. G. Kladas, "Modeling of interior permanent magnet machine using combined field-circuit analysis," in *Proc. ICEM*, 2010, pp. 1–6.

[13] K. Yamazaki and H. Ishigami, "Rotor-shape optimization of interior-permanent-magnet motors to reduce harmonic iron losses," *IEEE Trans. Ind. Electron.*, vol. 57, no. 1, pp. 61–69, Jan. 2010.

[14] D. Iles-Klumpner, M. Risticevic, and I. Boldea, "Advanced optimization design techniques for automotive interior permanent magnet synchronous machines," in *Proc. IEEE Int. Conf. Elect. Mach. Drives*, 2005, pp. 227–234.

[15] D. Iles-Klumpner and I. Boldea, "Comparative optimization design of an interior permanent magnet synchronous motor for an automotive active steering system," in *Proc. 35th Annu. IEEE Power Electron. Spec. Conf.*, Aachen, Germany, 2004, pp. 369–375.

[16] S.-H. Lee, J.-P. Hong, S.-M. Hwang, W.-T. Lee, J.-Y. Lee, and Y.-K. Kim, "Optimal design for noise reduction in interior permanent-magnet motor," *IEEE Trans. Ind. Appl.*, vol. 45, no. 6, pp. 1954–1960, Nov./Dec. 2009.

[17] J. Kwack, S. Min, and J.-P. Hong, "Optimal stator design of interior permanent magnet motor to reduce torque ripple using the level set method," *IEEE Trans. Magn.*, vol. 46, no. 6, pp. 2108–2111, Jun. 2010.

[18] S. Wu, D. D. Reigosa, Y. Shibukawa, M. A. Leetmaa, R. D. Lorenz, and Y. Li, "Interior permanent-magnet synchronous motor design for improving self-sensing performance at very low speed," *IEEE Trans. Ind. Appl.*, vol. 45, no. 6, pp. 1939–1946, Nov./Dec. 2009.

[19] P. Sergeant, F. De Belie, and J. Melkebeek, "Rotor geometry design of an interior permanent-magnet synchronous machine for more accurate sensorless control," in *Proc. ICEM*, 2010, pp. 1–6.

[20] X. Jannot, J.-C. Vannier, C. Marchand, M. Gabsi, J. Saint-Michel, and D. Sadarnac, "Multiphysic modeling of a high-speed interior permanent-magnet synchronous machine for a multiobjective optimal design," *IEEE Trans. Energy Convers.*, vol. 26, no. 2, pp. 457–467, Jun. 2011.

[21] M. Barcaro, N. Bianchi, and F. Magnussen, "Design considerations to maximize performance of an IPM motor for a wide flux-weakening region," in *Proc. ICEM*, 2010, pp. 1–7.

[22] G. Pellegrino and F. Cupertino, "IPM motor rotor design by means of FEA-based multi-objective optimization," in *Proc. IEEE ISIE*, 2010, pp. 1340–1346.

[23] G. Liuzzi, S. Lucidi, F. Parasiliti, and M. Villani, "Multi-objective optimization techniques for the design of induction motors," *IEEE Trans. Magn.*, vol. 39, no. 3, pp. 1261–1264, May 2003.

[24] W. L. Soong, S. Han, and T. M. Jahns, "Design of interior PM machine for field-weakening applications," in *Proc. Int. Conf. Elect. Mach. Syst.*, Oct. 8–11, 2007, pp. 654–664.

[25] D. Zarko, D. Ban, and T. A. Lipo, "Design optimization of interior permanent magnet motor with maximum torque output in the entire speed range," in *Proc. 2005 Eur. Conf. Power Electron. Appl.*, Dresden, Germany, 2005, pp. 1–10.

[26] J. F. Gieras and M. Wing, *Permanent Magnet Motor Technology*. New York: Marcel Dekker, 2002.

[27] W. I. Zangwill, "Nonlinear programming via penalty functions," *Manag. Sci.*, vol. 13, no. 5, pp. 344–358, Jan. 1967.

[28] G. Di Pillo and L. Grippo, "On the exactness of a class of nondifferentiable penalty functions," *J. Optim. Theory Appl.*, vol. 57, no. 3, pp. 399–410, Jun. 1988.

[29] W. L. Price, "Global optimization by controlled random search," *J. Optim. Theory Appl.*, vol. 40, no. 3, pp. 333–348, Jul. 1983.

[30] P. Brachetti, M. De Felice Ciccoli, G. Di Pillo, and S. Lucidi, "A new version of the Price's algorithm for global optimization," *J. Global Optim.*, vol. 10, no. 2, pp. 165–184, Mar. 1997.

Authorized licensed use limited to: Universita degli Studi di Roma La Sapienza. Downloaded on September 15,2022 at 09:42:33 UTC from IEEE Xplore. Restrictions apply.

[31] W. L. Price., "Global optimization algorithms for a CAD workstation," *J. Optim. Theory Appl.*, vol. 55, no. 1, pp. 133–146, Oct. 1987.
[32] A. Daidone, F. Parasiliti, M. Villani, and S. Lucidi, "A new method for the design optimization of three-phase induction motors," *IEEE Trans. Magn.*, vol. 34, no. 5, pp. 2932–2935, Sep. 1998.
[33] F. Parasiliti, M. Villani, S. Lucidi, and F. Rinaldi, "A new optimization approach for the design of IPM synchronous motor with wide constant-power region," in *Proc. ICEM*, 2010, pp. 1–7.

Francesco Parasiliti was born in Tortorici, Italy, in 1956. He received the M.S. degree in electrical engineering from the "Sapienza" University of Rome, Rome, Italy, in 1981.

In 1983, he joined the Department of Electrical and Information Engineering, University of L'Aquila, L'Aquila, Italy, as an Assistant Professor. From 1987 to 1988, he was a Research Fellow at the Swiss Federal Institute of Technology of Lausanne, Lausanne, Switzerland. From 1992 to 1999, he was an Associate Professor of Electrical Drives at the University of L'Aquila, where he has been a Full Professor since 2000. He has published more than 120 papers in scientific journals and conference proceedings. His studies deal with design optimization of induction, permanent-magnet synchronous, and reluctance motors, modeling and parameter observation of induction and synchronous machines, and digital control of electrical drives, including vector, sensorless, and fuzzy logic control.

Mr. Parasiliti is a member of the Steering Committee of the International Conference on Electrical Machines.

Marco Villani was born in Lecce, Italy, in 1960. He received the M.S. degree in electrical engineering from the University of L'Aquila, L'Aquila, Italy, in 1985.

In 1993, he joined the Department of Electrical and Information Engineering, University of L'Aquila, L'Aquila, Italy, as an Assistant Professor, teaching courses on power converters, electrical machines, and drives. In 1990, he was a Research Fellow at the University of Dresden, Dresden, Germany, and in 1995, at Nagasaki University, Nagasaki, Japan. In 1998, he cooperated in two EU-SAVE projects concerning energy efficiency improvements in three-phase induction motors. He is currently a Professor of Electrical Machines Design at the University of L'Aquila. His research interests are focused on modeling and simulation of electrical machines, energy saving in electric motors, optimization techniques for electrical machine designs, and design of permanent-magnet synchronous and reluctance motors. He is the author of more than 90 technical papers in scientific journals and conference proceedings.

Stefano Lucidi received the M.S. degree in electronic engineering from the "Sapienza" University of Rome, Rome, Italy, in 1980.

From 1982 to 1992, he was a Researcher at the Istituto di Analisi e dei Sistemi e Informatica, National Research Council of Italy. From September 1985 to May 1986, he was an Honorary Fellow of the Mathematics Research Center, University of Wisconsin, Madison. From 1992 to 2000, he was an Associate Professor of Operations Research at the "Sapienza" University of Rome, where he has been a Full Professor of Operations Research at the Department of Computer and System Sciences "Antonio Ruberti" since 2000 and the Director of the Ph.D. Program in Operations Research since November 2010. He teaches courses on operations research and global optimization methods in engineering management. His research interests are mainly focused on the study, definition, and application of nonlinear optimization methods and algorithms. His research activity has produced 72 papers published in international journals and 17 papers published in international books.

Francesco Rinaldi was born in Foggia, Italy, in 1980. He received the M.Sc. degree in computer engineering (*summa cum laude*) and the Ph.D. degree in operations research from the "Sapienza" University of Rome, Rome, Italy, in 2005 and 2009, respectively.

He is currently a Research Fellow in the Department of Computer and System Sciences "Antonio Ruberti," "Sapienza" University of Rome. His research interests include nonlinear optimization, data mining, and machine learning. He has published about ten papers in international journals.

Authorized licensed use limited to: Universita degli Studi di Roma La Sapienza. Downloaded on September 15,2022 at 09:42:33 UTC from IEEE Xplore. Restrictions apply.